

## Electrified Cloud Areas Observed in the SHV and LDR Radar Modes

VALERY MELNIKOV

*Cooperative Institute for Mesoscale Meteorological Studies, University of Oklahoma, and NOAA/OAR/National Severe Storms Laboratory, Norman, Oklahoma*

DUSAN S. ZRNIC

*NOAA/OAR/National Severe Storms Laboratory, Norman, Oklahoma*

MARK E. WEBER AND ALEXANDRE O. FIERRO

*Cooperative Institute for Mesoscale Meteorological Studies, University of Oklahoma, and NOAA/OAR/National Severe Storms Laboratory, Norman, Oklahoma*

DONALD R. MACGORMAN

*NOAA/OAR/National Severe Storms Laboratory, Norman, Oklahoma*

(Manuscript received 12 February 2018, in final form 16 October 2018)

### ABSTRACT

Strong in-cloud electric fields align ice particles that can be observed with polarization diversity radars. Radar data collected in the simultaneous transmission mode, wherein horizontally and vertically polarized waves are simultaneously transmitted and received (SHV), and in a mode whereby a single-polarization wave is transmitted and dual (orthogonal)-polarization waves are received simultaneously [linear depolarization (LDR) mode] are analyzed. The necessary time delay between the SHV and LDR modes for our radar was about 1–4 min. The data show that the areas of canted crystals from the LDR mode are larger than those from the SHV mode, thereby indicating that the LDR mode is more sensitive to canted ice cloud particles than the SHV mode. The data also demonstrate that the differential phase and correlation coefficient in the LDR mode are indicative of canted cloud crystals and that these variables often are more sensitive to canted crystals than the linear depolarization ratio studied earlier. Rapidly scanning radars such as those with a phased array antenna could operate sequentially in the SHV and LDR modes and thus better detect cloud volumes characterized by enhanced electric fields.

### 1. Introduction

Dual-polarization radars are capable of observing cloud areas of ice crystals canted by strong in-cloud electric fields. Such areas were first observed using radars with circular polarization (CP) (Hendry and McCormick 1976; Hendry and Antar 1982; Krehbiel et al. 1991, 1992, 1996, 2005; Metcalf 1995). It was shown that the correlation

coefficient and differential phase in the differential signal channel exhibited temporal alternations, which were related to abrupt changes in orientations of ice particles caused by electric fields. Strong depolarized signals have also been observed in satellite communication links when thunderstorms occurred along signal paths. Fast temporal variations in the signals have also been explained by alternations in orientation of cloud crystals caused by lightning changing in-cloud electric fields (e.g., Furuta et al. 1985 and citations therein). Caylor and Chandrasekar (1996) used radar with alternate polarizations to observe correlated temporal variations of the linear depolarization ratio  $L_{DR}$  and specific differential phase  $K_{DP}$ , which were attributed to changes in particles' orientations caused by electric fields. Ice particles align with a direction of an

---

Supplemental information related to this paper is available at the Journals Online website: <https://doi.org/10.1175/JTECH-D-18-0022.s1>.

---

*Corresponding author:* Valery Melnikov, [valery.melnikov@noaa.gov](mailto:valery.melnikov@noaa.gov)

DOI: 10.1175/JTECH-D-18-0022.1

© 2019 American Meteorological Society. For information regarding reuse of this content and general copyright information, consult the [AMS Copyright Policy](#) ([www.ametsoc.org/PUBSReuseLicenses](http://www.ametsoc.org/PUBSReuseLicenses)).

enhanced electric field, which typically have a significant vertical component. Such fields cant particles relative to their mean horizontal orientation in weak electric fields. Therefore, the terms *canted* and *aligned* are frequently used interchangeably in the literature on propagation of radar waves in thunderstorms.

Effects related to canted cloud crystals have also been observed by radars operating in the simultaneous mode, wherein horizontally and vertically polarized waves are simultaneously transmitted and received (SHV mode; Ryzhkov and Zrnić 2007; Hubbert et al. 2014a,b; Weber et al. 2017a; Biggerstaff et al. 2017). Differential reflectivity  $Z_{DR}$  and  $K_{DP}$  measured in the SHV mode may experience temporal and spatial variations, which are attributed to varying canting of ice cloud particles caused by varying in-cloud electric fields.

Canted ice crystals depolarize return radar signals. One can expect to observe the depolarization effects more clearly with radars operating in the circular polarization mode or in a mode in which a wave at a single-linear polarization is transmitted and waves at both orthogonal polarizations are simultaneously received [linear depolarization (LDR mode)]. In the LDR mode, the depolarized wave is not masked by a strong wave at the orthogonal polarization as it is in the SHV mode. One of the aims of our study is to compare the capabilities of detecting areas of canted ice crystals in the SHV and LDR modes. We also compare sensitivities of  $L_{DR}$ , the cross-polar correlation coefficient, and differential phase to detect areas of canted crystals.

The most popular polarization mode at present is the SHV, which has been recommended for a new generation of weather radars based on phased array antenna technology (Zrnić et al. 2007). The new weather radar should be capable of tracking aircrafts and making weather measurements simultaneously (e.g., Weber et al. 2017b). Electrified cloud areas are a hazard for aviation, military, and commercial space launch activities. Thus, the capability to detect such areas is important for aviation safety. Phased array radars could be capable of operating in different modes, including SHV, LDR, and CP. Here, radar data obtained in the SHV and LDR mode are analyzed to determine potential advantages of the LDR mode in detecting cloud areas of canted ice crystals.

## 2. Radar observations

From 2005 to 2008, the WSR-88D KOUN located in Norman, Oklahoma, could be switched between the SHV and LDR modes, with the switch between waveguides taking 1–4 min. In the SHV mode, reflectivity  $Z$ , Doppler velocity  $V$ , spectrum width  $W$ ,  $Z_{DR}$ , differential phase  $\Phi_{DP}$ , and copolar correlation coefficient  $\rho_{hh}$

were collected. In the LDR mode, fields of  $Z$ ,  $V$ ,  $W$ ,  $L_{DR}$ , differential phase  $\Phi_{XP}$ , and cross-polar correlation coefficient  $\rho_{xh}$  were collected. Equations for all these variables can be found, for instance, in Doviak and Zrnić (2006, section 8.5.2) and in Bringi and Chandrasekar (2001, section 2.3.3). To reduce noise influence in areas of weak signals, the lag-1 estimators of all polarimetric variables have been employed (Melnikov 2006; Melnikov and Zrnić 2007). With the lag-1 estimators, it is possible to obtain accurate polarimetric variables in larger cloud areas than with the traditional lag-0 estimators. This is because at low SNRs found in the cloud periphery, the traditional estimators can be biased by noise, whereas the lag-1 estimators are not. Sophisticated radial-by-radial noise estimation can be used to correct the traditional estimators (e.g., Ivić et al. 2014), but it is not done in this study for the sake of simplicity and rigor.

To compare the fields of radar variables, vertical cross sections (RHIs) through cores of thunderstorms were made in the SHV and LDR modes with a time delay of 1–4 min between the modes. This time is large in comparison with that of some electrification processes in thunderstorms, for example, lightning discharge, which can drastically alter the electric field distribution in a fraction of a second. Cloud polarization patterns can change on time scales from seconds to tens of minutes. On one hand, in radar observations by Metcalf (1995), Krehbiel et al. (1996, 2005), Caylor and Chandrasekar (1996), and Weber et al. (2017a), the changes in radar patterns occurred in tens of seconds. On the other hand, Biggerstaff et al. (2017) and Melnikov et al. (2009) observed radar patterns with a time scale of minutes. The  $K_{DP}$  patterns observed by Biggerstaff et al. (2017) lasted for tens of minutes. Clearly, the delay of 1–4 min between SHV and LDR in our observations will not support unambiguous conclusions on polarization pattern differences, which would be observed if the measurements were simultaneous. However, we believe that the consistent observations presented in this work provide credible evidence as to the enhanced sensitivity of the LDR mode in detecting volumes of electrically canted crystals.

An example of data from the SHV and LDR modes is shown in Fig. 1. The  $K_{DP}$  field (Fig. 1) exhibits a large area of negative values at the top of the thunderstorm, which indicates that ice particles were primarily vertically oriented. A contour of the area of negative  $K_{DP}$ , which is defined with a radial extent of at least 4 km having  $K_{DP} < -0.1^\circ \text{ km}^{-1}$ , is overlaid (black curve) on the other panels. The length of 4 km was chosen to be twice as long as the scale of  $K_{DP}$  calculations to reduce small-scale fluctuations in the  $K_{DP}$  values caused by nonuniform beam filling. The negative  $K_{DP}$  values in the

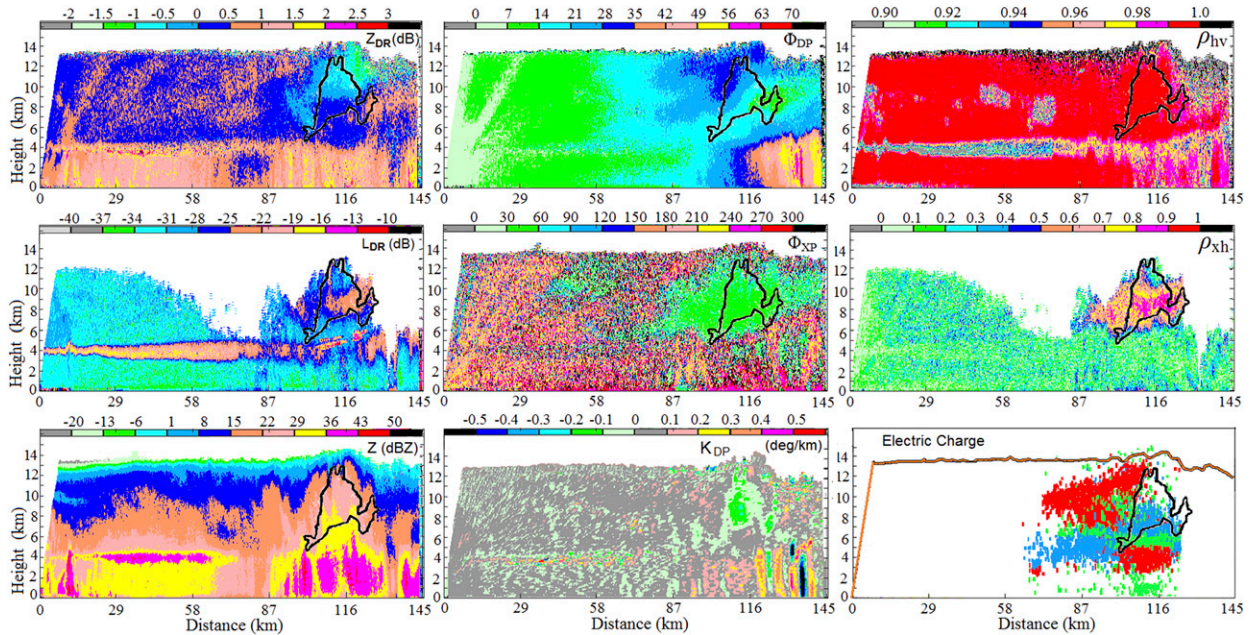


FIG. 1. RHIs collected on 26 Jun 2007 at (top) 1202 UTC in the SHV mode and (middle) 1205 UTC in the LDR mode at an azimuth of 209°. The outer contour of the negative  $K_{DP}$  area (the black contour) is superposed on the other fields for comparison. (bottom left) The  $Z$  field, and it is the same from both modes. (bottom center) The  $K_{DP}$  field is obtained in the SHV mode. (bottom right) The gross vertical electric charge structure inferred from the OKLMA VHF radiation source data along the same azimuth angle. The brown contour in this panel denotes the reflectivity echo boundary.

area suggest the presence of strong, vertically oriented electric fields in that area. The  $\rho_{hv}$  field is featureless, while both the  $L_{DR}$  and  $\rho_{xh}$  fields exhibit high values in that area, confirming the presence of canted crystals. Values of  $\Phi_{XP}$  fluctuate widely in rain and in areas where ice crystals are not preferentially aligned or fluttering. We explain this feature in section 3. In areas of canted crystals,  $\Phi_{XP}$  values fluctuate much less and exhibit more uniformity (the green areas in Fig. 1). Values of  $\Phi_{XP}$  depend on the shape and orientations of ice particles and the differential phase in the receiving path of the radar; this makes interpretation of  $\Phi_{XP}$  values difficult. To reveal areas with canted crystals, we look for areas with uniform  $\Phi_{XP}$  values. Combining the areas of high  $L_{DR}$  ( $\geq -25$  dB) and  $\rho_{xh}$  ( $\geq 0.5$ ) with that of uniform  $\Phi_{XP}$  (the green zone), we can conclude that LDR mode reveals a larger area of canted crystal than that obtained in the SHV mode. Similar situations are shown in the online supplemental material in Figs. S1–S3. Also, note a greenish area in the  $\Phi_{XP}$  panel (Fig. 1) in the trailing MCS at distances from 30 to 60 km and at heights over 10 km above the ground. We suggest that the electric field is sufficiently strong to cant the particles there. This area was not detected in the SHV mode.

In thunderstorms, graupel is frequently present above the melting layer along with ice crystals. Enhanced in-cloud electric fields can cant the crystals, but they have

no impact on graupel. In such cases, the  $L_{DR}$  values will have a contribution from the canted crystals that can be observable in the LDR mode. In the SHV mode, the radar variables will be heavily biased by graupel and the canted crystals cannot be observed.

Characteristics of the timing, development, and signal amplitude of the very high-frequency (VHF) radiation mapped by lightning mapping arrays, such as the one installed in Oklahoma (Thomas et al. 2001; MacGorman et al. 2008; Barth et al. 2015), can be used to identify which signals were received from lightning channels propagating through a negative charge region and which were from channels propagating through a positive charge region (Rison et al. 1999; Coleman et al. 2003; Rust et al. 2005; MacGorman et al. 1981, 2001, 2008). By mapping the sources produced in each charge region by many flashes over a period of several minutes, one can estimate the geometries of the ambient charge regions involved in lightning activity. Because the amplitude of VHF signals from channels propagating in negative charge tends to be much smaller than that from channels propagating in positive charge, the geometry of negative charge regions estimated by this technique is defined less clearly than the geometry of positive charge regions.

The gross charge structures within the thunderstorm obtained from the VHF Oklahoma Lightning Mapping

Array (OKLMA) exhibit a typical tripole (the bottom-right panel in Fig. 1). The positive (negative) charges are shown with red (blue) dots and unresolved charges are shown with green dots. The charge structure has been obtained from lightning flashes that occurred during the acquisition of radar data in the SHV and LDR modes.

The gross tripole charge structure evolves much more slowly than the local magnitudes of electric fields causing lightning initiation and represents a quasi-static configuration, with the largest electric field magnitudes on average being in the regions the text mentions. The charge increases in some part of that charge distribution (most likely the part near or adjacent to updrafts) until electrical breakdown occurs. The resulting lightning flash effectively neutralizes part of the charge in a positive region and part in a negative region, thereby causing a rapid change in the electric field, and the change would tend to be largest near the flash initiation point. Flash initiation points would tend to be distributed along the interfaces between the positive or negative charge or possibly above the uppermost charge region or below the lowermost charge region because electric field magnitudes tend to be larger just outside a charge region there than inside it. But each flash in a large storm would neutralize only a portion of the charge, so the orientation and magnitude of the field aligning the ice crystals will change.

A different situation is displayed in Fig. 2, where the  $Z_{DR}$  and  $\Phi_{DP}$  fields do not reveal canted particles. The variations in the  $Z_{DR}$  field at the top of the thunderstorm could be due to a mixture of particle habits, and some decrease in the  $Z_{DR}$  field at distances beyond about 90 km could be due to differential attenuation. The  $\Phi_{DP}$  field exhibits a typical pattern, where the phase increases with range, and there are no well-pronounced enhanced areas of negative  $K_{DP}$ . The  $\rho_{hv}$  field is featureless at the top. In contrast, the three polarimetric variables of the LDR mode point to the presence of canted particles at the top of the thunderstorm. Areas of enhanced  $L_{DR}$  and  $\rho_{xh}$  are well pronounced and fairly uniform areas of  $\Phi_{XP}$  are observed. This case supports the conclusion that the LDR mode is more sensitive to canted particles than the SHV mode. Similar cases are shown in Figs. S4–S6. Comparing the  $L_{DR}$ ,  $\Phi_{XP}$ , and  $\rho_{xh}$  fields, one can see that the extent of the  $\Phi_{XP}$  fields is larger than the extent of the other two. Thus,  $\Phi_{XP}$  is more sensitive to canted crystals than  $L_{DR}$  and  $\rho_{xh}$ .

We have analyzed 19 cases with observations in the LDR and SHV modes separated by a few minutes. In all these cases, areas of canted particles observed in the LDR mode were larger than those observed in the SHV mode. While our observations do not prove that LDR patterns are *always* larger than those from SHV mode if obtained simultaneously, we suggest that the consistency of the

above result strongly suggests that the LDR mode is more sensitive overall to areas of canted crystals than is SHV.

When comparing areas of variables obtained from the different modes, it is necessary to account for propagation effects. In the SHV mode, declining  $Z_{DR}$  values along a radial can be due to differential attenuation. In the LDR mode, incident radiation is depolarized in areas of canted crystals, so radiation beyond such areas contains a vertically polarized component coherent with the horizontally polarized wave. This component may increase the  $L_{DR}$  and  $\rho_{xh}$  from resolution volumes beyond the canted crystal region. If  $\rho_{xh}$  values increase along a radial (e.g., Figs. 1, 2, S2, and S3), then such areas contain canted crystals because depolarization increases. The extension of areas with canted crystals can also be estimated in a direction orthogonal to radar beams. Considering both features, we conclude that the LDR mode reveals larger areas of canted crystals than the SHV mode. Therefore, the LDR mode is more sensitive to the particles' alignment than the SHV mode because depolarized radiation in the LDR mode is not masked by a strong scattered wave at orthogonal polarization as it is in the SHV mode.

It is also evident from these data that the areas of canted crystals obtained from  $Z_{DR}$  and  $K_{DP}$  patterns in the SHV mode have spatial offsets that can be due to different sensitivities of these variables to canted crystals and to the propagation effects as well. The same holds for  $L_{DR}$ ,  $\Phi_{XP}$ , and  $\rho_{xh}$  variables in the LDR mode. Spatial offsets are also obvious for the variables from the SHV and LDR modes, which could be due to different sensitivities and also a time delay between the SHV and LDR observations. The spatial offsets point to a possibility of getting additional information on areas of canted crystals if the SHV and LDR variables are obtained simultaneously, for instance, with phased array radar as discussed later.

Areas of canted crystals in thunderstorms are often located above strong reflectivity cores (Figs. 1–3 and S1–S6), where appreciable updrafts exist. In several of the cases analyzed herein,  $Z_{DR}$  columns are also evident, reinforcing this conclusion. At the tops of thunderstorms, the updrafts diverge and become strongly turbulent as suggested by the observed large radar spectrum widths (Figs. S1–S7). The spectrum width shows the intensity of relative motions of scatterers. Electric field magnitudes in the thunderstorms must be sufficiently strong ( $\geq 50 \text{ kV m}^{-1}$ ) to align ice particles embedded in an intense turbulent flow.

The data in Figs. 1 and 2, and S1–S6 were collected in summer thunderstorms. Areas of uniform  $\Phi_{XP}$  and enhanced  $\rho_{xh}$  have also been observed with KOUN in winter storms. An example is in Fig. 3, where the  $L_{DR}$  field is almost featureless in the area of convection (at distances of 70–90 km), but the  $\Phi_{XP}$  and  $\rho_{xh}$  fields reveal

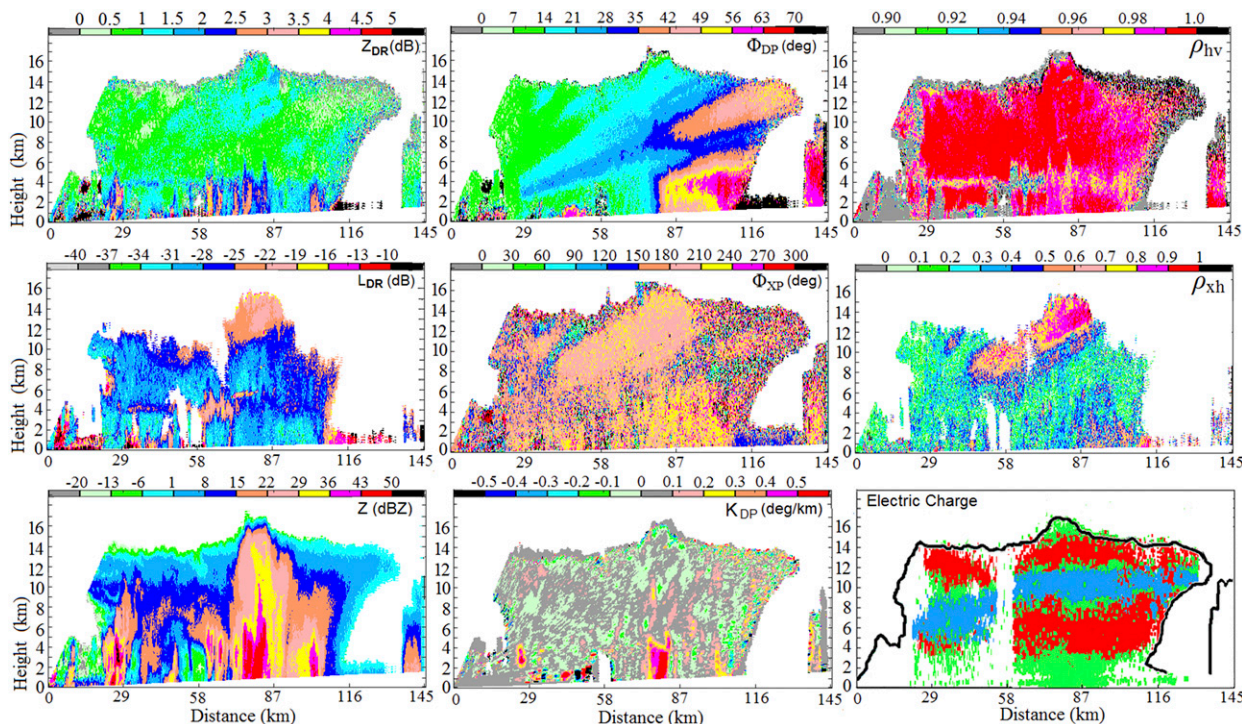


FIG. 2. As in Fig. 1, but at 1949 UTC (SHV mode) and 1953 UTC (LDR mode) 30 Jul 2007 at an azimuth of 329°.

canted particles, providing evidence of the presence of electric fields. The enhanced  $L_{DR}$  at heights 5–10 km at short distances from the radar are most likely due to large stellar/dendrite particles because the  $\Phi_{XP}$  and  $\rho_{xh}$  fields do not indicate the presence of canted particles.

It is possible to measure  $Z_{DR}$ ,  $\Phi_{DP}$ ,  $\rho_{hv}$ ,  $L_{DR}$ ,  $\Phi_{XP}$ , and  $\rho_{xh}$  simultaneously using radar that employs a mode with alternate transmission of horizontally and vertically polarized waves (AHV mode) and simultaneous reception of both polarizations (e.g., Zrnić 1991; Bringi and Chandrasekar 2001, section 6.4.3). This mode cannot be used for long-range surveillance at low elevation angles

because of the low pulse repetition frequency (PRF) that would be needed to cover large distances, which on the WSR-88D is over 450 km. Low PRFs reduce the correlation between radar samples, thus degrading the quality of polarimetric variables (Melnikov and Zrnić 2015). To achieve acceptable error estimates, the PRF should be about 1000 Hz at S-band frequency in the AHV mode. Such a PRF could be utilized at higher antenna elevations, where data are collected over significantly shorter distances. Another approach to obtain all polarimetric variables would be to switch between the SHV and LDR modes at high antenna elevations.

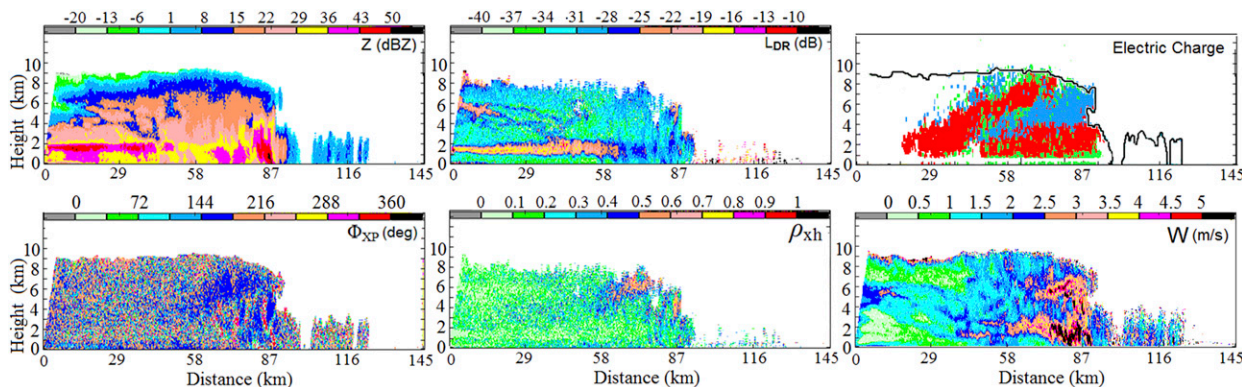


FIG. 3. RHIs in the LDR mode collected in a winter storm at 0525 UTC 13 Feb 2007 at an azimuth of 158°.

In such a case, the best estimates of all polarimetric variables can be obtained. Observations to short ranges in the LDR mode could be used to obtain information about the particles' alignment near thunderstorm tops. Both options, and possible other alternatives, might yield better information about areas of canted crystals. Consideration of these, however, is beyond the scope of this study.

### 3. Theoretical considerations

Consider  $\rho_{\text{xh}}$  values in areas of canted crystals. The geometry of scattering for the LDR mode is shown in Fig. 4, where the incident radar wave  $E$  (red) is polarized, as on KOUN, in the horizontal plane. The incidence direction designated by the vector  $\mathbf{k}$  makes the angle  $\gamma$  with the horizontal plane, where  $\gamma$  is the elevation angle of the radar antenna. The orientation of the ice crystal is characterized by two angles: the canting angle  $\theta$  and the azimuthal angle  $\varphi$ . In weak electric fields, the crystal flutters in the air, so angle  $\varphi$  varies in the interval  $0^\circ$ – $360^\circ$  and the mean canting angle is  $0^\circ$ .

A scatterer depolarizes the horizontally polarized incident wave; the scattered wave therefore contains both horizontally and vertically polarized components. The amplitudes of these waves are proportional to the scattering matrix elements  $S_{\text{hh}}$  and  $S_{\text{vh}}$  [e.g., [Bringi and Chandrasekar 2001](#), Eq. (2.53)], defined as

$$S_{\text{hh}} = \alpha_{\text{h}} + \Delta\alpha \sin^2\theta \sin^2\varphi, \quad \Delta\alpha = \alpha_{\text{v}} - \alpha_{\text{h}}, \quad (1a)$$

$$S_{\text{vh}} = \Delta\alpha (\sin\gamma \sin^2\theta \sin\varphi \cos\varphi + \cos\gamma \sin\theta \cos\theta \sin\varphi), \quad (1b)$$

where  $\alpha_{\text{h}}$  and  $\alpha_{\text{v}}$  are polarizabilities of the particle in the horizontal and vertical directions, respectively, at horizontal orientation of the particle. The correlation function  $R_{\text{xh}}$  for the scattered waves is  $R_{\text{xh}} = \langle S_{\text{hh}}^* S_{\text{vh}} \rangle$ , where the angle brackets stand for temporal/ensemble averaging and the asterisk denotes complex conjugate. Therefore,

$$R_{\text{xh}} = \frac{1}{2} \langle \alpha_{\text{h}}^* \Delta\alpha (\sin\gamma \sin^2\theta \sin 2\varphi + \cos\gamma \sin 2\theta \sin\varphi) + \frac{1}{2} \langle |\Delta\alpha|^2 (\sin\gamma \sin^4\theta \sin^2\varphi \sin 2\varphi + \cos\gamma \sin^2\theta \sin 2\theta \sin^3\varphi) \rangle, \quad (2a)$$

$$\Phi_{\text{XP}} = \arg(R_{\text{xh}}), \quad \rho_{\text{xh}} = |R_{\text{xh}}| / (\langle |S_{\text{hh}}|^2 \rangle \langle |S_{\text{vh}}|^2 \rangle)^{1/2}, \quad (2b)$$

$$L_{\text{DR}} = 10 \log(\langle |S_{\text{vh}}|^2 \rangle / \langle |S_{\text{hh}}|^2 \rangle). \quad (2c)$$

If electric fields are not strong enough to affect the alignment of ice particles, then the angles  $\theta$  and  $\varphi$  vary independently and, because  $\varphi$  varies from  $0^\circ$  to  $360^\circ$ ,  $R_{\text{xh}} = 0$  and correspondingly  $\rho_{\text{xh}} = 0$ , which is the intrinsic

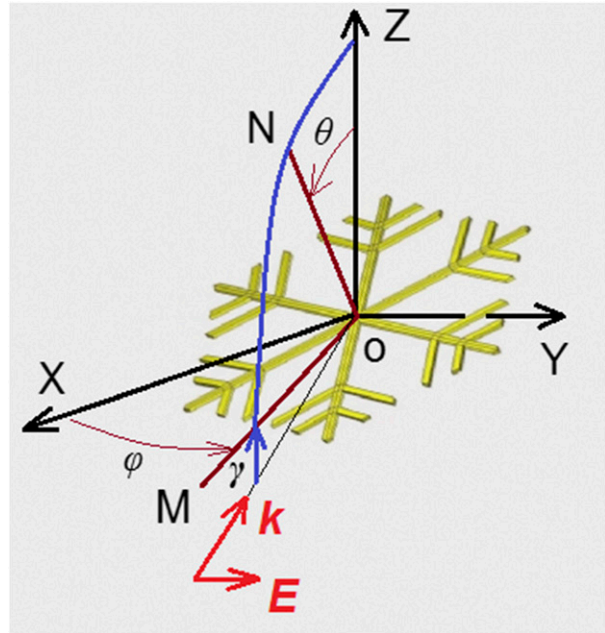


FIG. 4. Orientation of the ice particle (yellow) in the coordinate system (black) centered at the radar resolution volume. The plane  $XOY$  is horizontal. The line  $ON$  is orthogonal to the plane of the particle. The canting angle is  $\theta$ . The line  $OM$  lies in the horizontal plane. The incident radar wave is polarized in the horizontal plane. The incident direction makes the angle  $\gamma$  with the horizontal plane.

$\rho_{\text{xh}}$ . Radar data show that in weak electric fields  $\rho_{\text{xh}} = 0.2$ – $0.3$ . This positive bias is a consequence of a finite number of samples used in the estimation ([Melnikov 2006](#)). At zero intrinsic  $\rho_{\text{xh}}$ , the phase  $\Phi_{\text{XP}}$  fluctuates widely, as is observed in radar data. The  $\Phi_{\text{XP}}$ ,  $L_{\text{DR}}$ , and  $\rho_{\text{xh}}$  values differently depend on  $S_{\text{hh}}$  and  $S_{\text{vh}}$  [see Eqs. (2b) and (2c)], which in turn depend on the crystals' habits, orientations, direction of electric forces, and angle of incident radiation. Therefore, radar patterns relevant to canted particles do not frequently coincide. Features in  $Z_{\text{DR}}$  and  $K_{\text{DP}}$  fields also frequently exhibit spatial offsets, which is also explained by their different dependences on various parameters. For instance,  $K_{\text{DP}}$  depends on number concentration of scatterers, but  $Z_{\text{DR}}$  does not.

An enhanced electric field reorients a particle so that the axis along the particles' longest dimension aligns with the field, thus dampening variations in  $\varphi$  and  $\theta$ : the stronger the field, the smaller the variations in  $\varphi$  and  $\theta$ . This is why the intrinsic  $\rho_{\text{xh}}$  coefficient increases in electric fields. The phase  $\Phi_{\text{XP}}$  is the argument of  $R_{\text{xh}}$  and can have various values depending on the mean  $\theta$  and  $\varphi$  and on the radar viewing angle. Therefore, it is challenging to relate the measured  $\Phi_{\text{XP}}$  to the microphysical properties of ice crystals. But areas with low fluctuating phases can reveal canted particles. The high  $\rho_{\text{xh}}$  values and the uniformity of  $\Phi_{\text{XP}}$  areas follow from damped

variations in the  $\varphi$  angle. The spatial variability of the electric field vector's orientation impacts the values of  $\rho_{\text{xh}}$  and  $\Phi_{\text{XP}}$  as well.

The linear depolarization ratio strongly depends on the sizes and habits of ice particles and on their orientations. That is why large  $L_{\text{DR}}$  cannot be directly attributed to canted crystals. The  $\Phi_{\text{XP}}$  and  $\rho_{\text{xh}}$  strongly depend on the orientations of crystals and therefore are better indicators of canted particles than  $L_{\text{DR}}$ .

To obtain the correlation function  $R_{\text{hv}}$  in the SHV mode, the  $S_{\text{hh}}$  element [Eq. (1a)] of the scattering matrix should be correlated with the element  $S_{\text{vv}}$ :

$$S_{\text{vv}} = \alpha_{\text{h}} + \Delta\alpha(\sin\gamma \sin\theta \cos\varphi + \cos\gamma \cos\theta)^2. \quad (3)$$

Then,  $R_{\text{hv}} = \langle S_{\text{hh}}^* S_{\text{vv}} \rangle$  and for random  $\varphi$  we obtain

$$R_{\text{hv}} = \langle |\alpha_{\text{h}}|^2 \rangle + \text{Re}(\langle \alpha_{\text{h}} \Delta\alpha^* \rangle) C_1 + j \text{Im}(\langle \alpha_{\text{h}} \Delta\alpha^* \rangle) C_2 + \langle |\Delta\alpha|^2 \rangle C_3, \quad (4)$$

$$\Phi_{\text{DP}} = \arg(R_{\text{hv}}), \quad \rho_{\text{hv}} = |R_{\text{hv}}| / (\langle |S_{\text{hh}}|^2 \rangle \langle |S_{\text{vv}}|^2 \rangle)^{1/2}, \quad (5)$$

$$C_1 = 1 - J_1/2 + (3J_1/2 - 1) \sin^2 \gamma, \quad (6a)$$

$$C_2 = (1 - 3J_1/2) \cos^2 \gamma, \quad (6b)$$

$$C_3 = e^{-j\psi_t} \cos\psi_t [J_1 - J_2 + (5J_2/4 - J_1) \sin^2 \gamma], \quad (6c)$$

$$J_1 = \langle \sin^2 \theta \rangle, \quad J_2 = \langle \sin^4 \theta \rangle, \quad (6d)$$

where  $\psi_t$  is the differential phase upon transmission (Melnikov 2017). Phase  $\psi_t$  was close to  $27^\circ$  in KOUN in 2006–08. For a circular polarization,  $\psi_t = \pm 90^\circ$  and  $C_3 = 0$ . In such a case, the modulus of  $R_{\text{hv}}$  decreases and  $\rho_{\text{hv}}$  decreases. A decrease in  $\rho_{\text{hv}}$  at switching polarizations from linear  $45^\circ$ —that is, the in-phase SHV—to circular polarization was observed by Krehbiel et al. (2005). It follows from Eq. (5) that  $\rho_{\text{hv}}$  exceeds 0.8 for ice particles regardless of their orientations and phase  $\psi_t$ . This is the main reason why high correlation coefficients are observed in clouds in the SHV mode and  $\rho_{\text{hv}}$  fields are featureless in areas of canted ice particles.

#### 4. Discussion and conclusions

Canted ice cloud particles depolarize scattered and propagated electromagnetic waves. Areas of canted cloud crystals can be detected in both the simultaneous transmit (SHV) and linear depolarization (LDR) radar modes. The radar data presented here show that the LDR mode detects larger areas of canted crystals than the SHV mode does. The LDR mode is therefore more sensitive to canted

crystals. Canted crystals are detected in the SHV mode in areas of well-pronounced negative  $K_{\text{DP}}$ . Fields of copolar correlation coefficient  $\rho_{\text{hv}}$  are typically featureless in those areas. In the LDR mode, all polarimetric variables—that is,  $L_{\text{DR}}$ ,  $\Phi_{\text{XP}}$ , and  $\rho_{\text{xh}}$ —are sensitive to canted crystals, with the enhanced values of  $\rho_{\text{xh}}$  and  $L_{\text{DR}}$  and the values of the phase  $\Phi_{\text{XP}}$  remaining somewhat uniform in areas of canted particles. This is in contrast to areas of fluttering crystals, where  $\Phi_{\text{XP}}$  fluctuates widely. Frequently, areas of high  $\rho_{\text{xh}}$  and uniform  $\Phi_{\text{XP}}$  are often larger than areas of enhanced  $L_{\text{DR}}$ , indicating that  $\rho_{\text{xh}}$  and  $\Phi_{\text{XP}}$  are more sensitive to canted crystals than  $L_{\text{DR}}$ . The main source of this feature is damped variations of particles' orientations caused by in-cloud electric fields. The values of  $\rho_{\text{xh}}$  and  $\Phi_{\text{XP}}$  also depend on the spatial variability of the orientation of the enhanced electric field vector.

The reason why the LDR mode is more sensitive to canted crystals than the SHV mode is that the depolarized radar wave in the LDR mode is not masked by a strong backscattered wave at the same polarization as it is in the SHV mode. The presented data show the advantages of the LDR mode in observing areas of canted ice particles within summer and winter thunderstorms. Therefore, a combination of data obtained in the SHV and LDR modes could help to shed more light on electric processes in clouds.

The gross charge structures in the analyzed cases exhibit a typical tripole, which consists of a main negative charge at midlevels sandwiched in between two layers of positive charge. Areas of canted crystals are frequently observed near the tops of thunderstorms, likely near or above the interface between the main midlevel negative charge region and the upper positive charge region, where in-cloud electric field magnitudes often are large ( $\geq 50 \text{ kV m}^{-1}$ ; e.g., Marshall et al. 1995; MacGorman and Rust 1998; Mansell et al. 2010; Fierro et al. 2013). Near the top of thunderstorms, the updrafts diverge and become strongly turbulent as evidenced from the spectrum width fields. Turbulence disorders the orientations of ice particles. Electric fields in thunderstorms have to be of certain strength to align ice particles in intense turbulence. Turbulent air contains eddies of various sizes, which affect particles' orientations differently. Cho et al. (1981) and Weinheimer and Few (1987) considered the orientations of pristine ice particles in turbulent air in electric fields. They concluded that the turbulence of scales close to the Kolmogorov's microscale weakly affects orientations of ice particles. Larger turbulent vortices also affect the orientations: ice particles should be oriented orthogonal to the main air motion as in their free fall. The main turbulent velocity can be of any direction and creates torque that must be compared with electric torque.

Klett (1995) estimated the variance in the orientations of pristine ice particles for the Kolmogorov spectrum of eddies in the absence of electric forces. To obtain dependencies of the orientations on electric fields in thunderstorms, radar data along with measurements of the in-cloud fields should be analyzed. Measurements of polarimetric variables of the SHV and LDR modes would be beneficial for cloud physics, atmospheric electricity, and aviation safety.

Possible future deployment of operational phased array weather radar could deliver information on aircraft and weather simultaneously (Stailey and Hondl 2016). The detection of electrified cloud areas is critical for aviation safety. While the main data collection mode for the new radar would likely be SHV, polarimetric variables in LDR mode could be obtained in order to better detect electrified areas. Arguably, the alternate polarization mode could be envisaged as an option for that, but the best quality of radar variables is obtained in the genuine SHV and LDR modes. The LDR mode could be operated for a short period of time near cloud tops. Obtaining all polarimetric variables with a good quality would enhance the capability of the new radar to detect areas of ice crystals canted by strong in-cloud electric fields. Note that it will be necessary to account for the cross-polarization introduced by phased array antenna element patterns when the beam is scanned out of the principal planes. Array calibration and polarization correction techniques are a major thrust of ongoing polarimetric phased array radar research and will be critical in achieving the capabilities discussed in this paper.

*Acknowledgments.* We thank Drs. Paul Krehbiel, Terry Schuur, and Edward Mansell for their valuable comments. We also thank the anonymous reviewers for their comments, which helped to improve the paper. Funding for this study was provided in part by the NOAA/Office of Oceanic and Atmospheric Research under NOAA–University of Oklahoma Cooperative Agreement NA17RJ1227, U.S. Department of Commerce.

#### REFERENCES

- Barth, M. C., and Coauthors, 2015: The Deep Convective Clouds and Chemistry (DC3) Field Campaign. *Bull. Amer. Meteor. Soc.*, **96**, 1281–1309, <https://doi.org/10.1175/BAMS-D-13-00290.1>.
- Biggerstaff, M., Z. Zounes, A. Alford, G. Carrie, J. T. Pilkey, M. Uman, and D. Jordan: 2017: Flash propagation and inferred charge structure relative to radar-observed ice alignment signatures in a small Florida mesoscale convective system. *Geophys. Res. Lett.*, **44**, 8027–8036, <https://doi.org/10.1002/2017GL074610>.
- Bringi, V. N., and V. Chandrasekar, 2001: *Polarimetric Doppler Weather Radar: Principles and Applications*. Cambridge University Press, 636 pp., <https://doi.org/10.1017/CBO9780511541094>.
- Caylor, I. J., and V. Chandrasekar, 1996: Time-varying ice crystal orientation in thunderstorms observed with multiparameter radar. *IEEE Trans. Geosci. Remote Sens.*, **34**, 847–858, <https://doi.org/10.1109/36.508402>.
- Cho, H.-R., J. V. Iribarne, and W. G. Richards, 1981: On the orientations of ice crystals in a cumulonimbus cloud. *J. Atmos. Sci.*, **38**, 1111–1114, [https://doi.org/10.1175/1520-0469\(1981\)038<1111:OTOOIC>2.0.CO;2](https://doi.org/10.1175/1520-0469(1981)038<1111:OTOOIC>2.0.CO;2).
- Coleman, L. M., T. C. Marshall, M. Stolzenburg, T. Hamlin, P. R. Krehbiel, W. Rison, and R. J. Thomas, 2003: Effects of charge and electrostatic potential on lightning propagation. *J. Geophys. Res.*, **108**, 4298, <https://doi.org/10.1029/2002JD002718>.
- Doviak, R. J., and D. S. Zrnić, 2006: *Doppler Radar and Weather Observations*. 2nd ed. Academic Press, 562 pp.
- Fierro, A. O., E. R. Mansell, C. Ziegler, and D. R. MacGorman, 2013: The implementation of an explicit charging and discharge lightning scheme within the WRF-ARW model: Benchmark simulations with a continental squall line and a tropical cyclone. *Mon. Wea. Rev.*, **141**, 2390–2415, <https://doi.org/10.1175/MWR-D-12-00278.1>.
- Furuta, O., H. Yuki, and M. Yamada, 1985: Abrupt changes in cross polarization observed during thunder. *IEEE Trans. Antennas Propag.*, **33**, 625–632, <https://doi.org/10.1109/TAP.1985.1143635>.
- Hendry, A., and G. C. McCormick, 1976: Radar observation of the alignment of precipitation particles by electrostatic fields in thunderstorms. *J. Geophys. Res.*, **81**, 5353–5357, <https://doi.org/10.1029/JC081i030p05353>.
- , and Y. M. M. Antar, 1982: Radar observations of polarization characteristics and lightning-induced realignment of atmospheric ice crystals. *Radio Sci.*, **17**, 1243–1250, <https://doi.org/10.1029/RS017i005p01243>.
- Hubbert, J. C., S. M. Ellis, W.-Y. Chang, S. Rutledge, and M. Dixon, 2014a: Modeling and interpretation of S-band ice crystal depolarization signatures from data obtained by simultaneously transmitting horizontally and vertically polarized fields. *J. Appl. Meteor. Climatol.*, **53**, 1659–1677, <https://doi.org/10.1175/JAMC-D-13-0158.1>.
- , —, —, and Y.-C. Liou, 2014b: X-band polarimetric observations of cross coupling in the ice phase of convective storms in Taiwan. *J. Appl. Meteor. Climatol.*, **53**, 1678–1695, <https://doi.org/10.1175/JAMC-D-13-0360.1>.
- Ivić, I. R., J. C. Krause, O. E. Boydston, A. E. Daniel, A. D. Free, and W. D. Zittel, 2014: Effects of radial-based noise power estimation on spectral moment estimates. *J. Atmos. Oceanic Technol.*, **31**, 2671–2691, <https://doi.org/10.1175/JTECH-D-14-00048.1>.
- Klett, J. D., 1995: Orientation model for particles in turbulence. *J. Atmos. Sci.*, **52**, 2276–2285, [https://doi.org/10.1175/1520-0469\(1995\)052<2276:OMFPIT>2.0.CO;2](https://doi.org/10.1175/1520-0469(1995)052<2276:OMFPIT>2.0.CO;2).
- Krehbiel, P. R., W. Rison, S. McCrary, T. Blackman, and M. Brook, 1991: Dual-polarization radar observations of lightning echoes and precipitation alignment at 3-cm wavelength. Preprints, *25th Int. Conf. on Radar Meteorology*, Paris, France, Amer. Meteor. Soc., 901–904.
- , T. Chen, S. McCrary, W. Rison, G. Gray, T. Blackman, and M. Brook, 1992: Dual polarization radar signatures of the potential for lightning in electrified storms. *Proceedings: 9th International Conference on Atmospheric Electricity*, A. I. Voikov Main Geophysical Observatory, 166–169.
- , —, —, —, —, and M. Brook, 1996: The use of dual channel circular-polarization radar observations for remotely sensing storm electrification. *Meteor. Atmos. Phys.*, **59**, 65–82, <https://doi.org/10.1007/BF01032001>.

- , and Coauthors, 2005: Lightning and dual-polarization radar structure of small convective storms. *32nd Conf. Radar Meteorology*, Albuquerque, NM, Amer. Meteor. Soc., 15R.2, <https://ams.confex.com/ams/32Rad11Meso/webprogram/Paper96952.html>.
- MacGorman, D. R., and W. D. Rust, 1998: *The Electrical Nature of Storms*. Oxford University Press, 422 pp.
- , A. A. Few, and T. L. Teer, 1981: Layered lightning activity. *J. Geophys. Res.*, **86**, 9900–9910, <https://doi.org/10.1029/JC086iC10p09900>.
- , J. M. Straka, and C. L. Ziegler, 2001: A lightning parameterization for numerical cloud models. *J. Appl. Meteor.*, **40**, 459–478, [https://doi.org/10.1175/1520-0450\(2001\)040<0459:ALPNC>2.0.CO;2](https://doi.org/10.1175/1520-0450(2001)040<0459:ALPNC>2.0.CO;2).
- , and Coauthors, 2008: TELEX: The Thunderstorm Electrification and Lightning Experiment. *Bull. Amer. Meteor. Soc.*, **89**, 997–1013, <https://doi.org/10.1175/2007BAMS2352.1>.
- Mansell, E. R., C. L. Ziegler, and E. C. Bruning, 2010: Simulated electrification of a small thunderstorm with two-moment bulk microphysics. *J. Atmos. Sci.*, **67**, 171–194, <https://doi.org/10.1175/2009JAS2965.1>.
- Marshall, T. C., M. P. McCarthy, and W. D. Rust, 1995: Electric field magnitudes and lightning initiation in thunderstorms. *J. Geophys. Res.*, **100**, 7097–7103, <https://doi.org/10.1029/95JD00020>.
- Melnikov, V. M., 2006: One-lag estimators for cross-polarization measurements. *J. Oceanic Atmos. Technol.*, **23**, 915–926, <https://doi.org/10.1175/JTECH1919.1>.
- , 2017: Parameters of ice particles retrieved from radar data. *J. Oceanic Atmos. Technol.*, **34**, 717–728, <https://doi.org/10.1175/JTECH-D-16-0123.1>.
- , and D. S. Zrnić, 2007: Autocorrelation and cross-correlation estimators of polarimetric variables. *J. Atmos. Oceanic Technol.*, **24**, 1337–1350, <https://doi.org/10.1175/JTECH2054.1>.
- , and —, 2015: On the alternate transmission mode for polarimetric phased array weather radar. *J. Oceanic Atmos. Technol.*, **32**, 220–233, <https://doi.org/10.1175/JTECH-D-13-00176.1>.
- , T. Schuur, and A. Ryzhkov, 2009: Recognition of lightning echoes with the polarimetric WSR-88D. *34th Conf. on Radar Meteorology*, Williamsburg, VA, Amer. Meteor. Soc., P13.8, <https://ams.confex.com/ams/34Radar/webprogram/Paper155320.html>.
- Metcalfe, J. I., 1995: Radar observations of changing orientations of hydrometeors in thunderstorms. *J. Appl. Meteor.*, **34**, 757–772, [https://doi.org/10.1175/1520-0450\(1995\)034<0757:ROOCOO>2.0.CO;2](https://doi.org/10.1175/1520-0450(1995)034<0757:ROOCOO>2.0.CO;2).
- Rison, W., R. J. Thomas, P. R. Krehbiel, T. Hamlin, and J. Harlin, 1999: A GPS-based three-dimensional lightning mapping system: Initial observations in central New Mexico. *Geophys. Res. Lett.*, **26**, 3573–3576, <https://doi.org/10.1029/1999GL010856>.
- Rust, W. D., and Coauthors, 2005: Inverted-polarity electrical structures in thunderstorms in the Severe Thunderstorm Electrification and Precipitation Study (STEPS). *Atmos. Res.*, **76**, 247–271, <https://doi.org/10.1016/j.atmosres.2004.11.029>.
- Ryzhkov, A., and D. Zrnić, 2007: Depolarization in ice crystals and its effect on radar polarimetric measurements. *J. Atmos. Oceanic Technol.*, **24**, 1256–1267, <https://doi.org/10.1175/JTECH2034.1>.
- Stailey, J. E., and K. D. Hondl, 2016: Multifunction phased array radar for aircraft and weather surveillance. *Proc. IEEE*, **104**, 649–659, <https://doi.org/10.1109/JPROC.2015.2491179>.
- Thomas, R. J., P. R. Krehbiel, W. Rison, T. Hamlin, J. Harlin, and D. Shown, 2001: Observations of VHF source powers radiated by lightning. *Geophys. Res. Lett.*, **28**, 143–146, <https://doi.org/10.1029/2000GL011464>.
- Weber, M. E., D. Zrnić, and P. Zhang, 2017a: High temporal-resolution monitoring of ice crystal alignment. *33rd Conf. on Environmental Information Processing Technologies*, Seattle, WA, Amer. Meteor. Soc., 8A.3, <https://ams.confex.com/ams/97Annual/webprogram/Paper309454.html>.
- , J. Y. Cho, and H. G. Thomas, 2017b: Command and control for multifunction phased array radar. *IEEE Trans. Geosci. Remote Sens.*, **55**, 5899–5912, <https://doi.org/10.1109/TGRS.2017.2716935>.
- Weinheimer, A. J., and A. A. Few, 1987: The electric field alignment of ice particles in thunderstorms. *J. Geophys. Res.*, **92**, 14 833–14 844, <https://doi.org/10.1029/JD092iD12p14833>.
- Zrnić, D. S., 1991: Complete polarimetric and Doppler measurements with a single receiver radar. *J. Atmos. Oceanic Technol.*, **8**, 159–165, [https://doi.org/10.1175/1520-0426\(1991\)008<0159:CPADMW>2.0.CO;2](https://doi.org/10.1175/1520-0426(1991)008<0159:CPADMW>2.0.CO;2).
- , and Coauthors, 2007: Agile-beam phased array radar for weather observations. *Bull. Amer. Meteor. Soc.*, **88**, 1753–1766, <https://doi.org/10.1175/BAMS-88-11-1753>.